# Journal of Materials Chemistry C

Accepted Manuscript


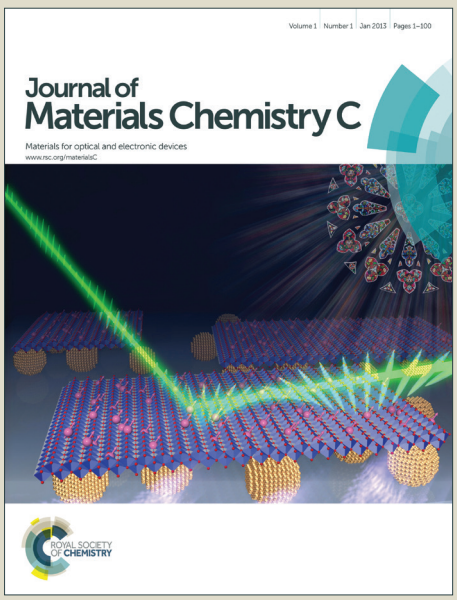





ROYAL SOCIETY OF CHEMISTRY

www.rsc.org/materialsC

Cite this: DOI: 10.1039/c0xx00000x

www.rsc.org/xxxxxx

ARTICLE TYPE

# Sub-10 nm and monodisperse $\beta$-$NaYF_4$:Yb,Tm,Gd nanocrystals with intense ultraviolet upconversion luminescence

**Feng Shi and Yue Zhao***

***Received (in XXX, XXX) Xth XXXXXXXXX 20XX, Accepted Xth XXXXXXXXX 20XX***

**DOI: 10.1039/b000000x**

Despite the fast progress in lanthanide-doped upconversion nanocrystals (UCNCs), the preparation of ultra-small, monodisperse and uniform UCNCs with intense high-order ultraviolet upconversion luminescence (UV UCL) is still a challenging issue. Here we report on a method for the controlled synthesis of $\beta$-$NaYF_4$:18%Yb,0.5%Tm,X%Gd NCs, with sizes ranging from 8 nm to 25 nm in diameter. We show that under 980 nm excitation, 5-photon UCL (291 nm and 345 nm) from the $^1I_6$ level of $Tm^{3+}$ is more intense than the 4-photon UCL (363 nm and 451 nm) from the $^1D_2$ level and the 3-photon UCL (474 nm) from the $^1G_4$ level of $Tm^{3+}$. Specifically, when the particle size decreases to 8 nm, intense UV UCL from $Tm^{3+}$ and high-order UV UCL from $Gd^{3+}$ are still observed. Moreover, core/shell $\beta$-$NaYF_4$:18%Yb,0.5%Tm,20%Gd@$NaGdF_4$ NCs of 12 nm in diameter were also synthesized, exhibiting more efficient UCL than the 8 nm diameter-core NCs. Ultra-small UCNCs with intense UV UCL are promising for biomedical applications.

## Introduction

Lanthanide-doped upconversion nanocrystals (UCNCs) are capable of converting low-energy near-infrared (NIR) photons into high-energy visible and ultraviolet photons via the multiphoton processes.[1-4] Intensive research effort has been made on these UCNCs that have potential for many applications such as bioimaging, displays, phototherapy and photocatalysis, due to their unique properties including tunable multicolor emission, deep tissue penetration, non-blinking, suppression of autofluorescence and low *in vitro* and *in vivo* toxicity.[5-11] Recently, the use of UCNCs has also been proposed as a general means to enable NIR light-controlled release of payloads from UV-sensitive polymer nanocarriers or hydrogels.[12-14] By loading UCNCs within UV-sensitive systems, upon NIR excitation, the nanoparticles act as an inside UV light source and emitted UV photons can be absorbed by the photosensitive polymer, thus activating the photochemical reaction and leading to the polymer carrier's disintegration. The use of NIR instead of UV light excitation is important for light-controlled biomedical applications due to enhanced tissue penetration and less damage on healthy cells.[15-17] In this specific application context, small-sized UCNCs are highly desired because their encapsulation by UV-sensitive polymer nanocarriers (e.g., micelles and vesicles) may be easier than the usually used large particles.[12-14] Therefore, it is of interest to develop synthetic methods giving easy access to ultra-small UCNCs that display efficient upconversion emission in the UV region upon NIR excitation.

Among the many UCNCs, $\beta$-$NaYF_4$ has been regarded as one of the most efficient host materials, being several orders of magnitude more efficient than $\alpha$-$NaYF_4$.[7, 18-21] The application of lanthanide-doped $\beta$-$NaYF_4$ UCNCs in biomedicine has been growing rapidly and offers excellent prospects for the development of new non-invasive strategies for the bioimaging *in vivo* and cancer therapy.[8, 10] To date, a great deal of effort has been devoted to the preparation of $\beta$-$NaYF_4$ through hydrothermal synthesis, co-precipitation, ionic liquids (ILs)-based synthesis and solvothermal method.[21-26] Though successful in many respects, those synthetic methods all have their respective limitations. For instance, the hydrothermal approach is believed to be an effective water-based method for the synthesis of UCNCs under relative low temperatures, allowing for the preparation of various kinds of well-crystallized UCNCs with fine control of size, shape and structure. However, it is hard to produce ultra-small (less than 10 nm) and monodisperse UCNCs. Co-precipitation methods are simple, but it is necessary to improve the crystallinity of the nanoparticles by post-synthesis treatments. As for ILs, their attractive properties such as thermal and chemical stability, and negligible vapor pressure have been applied in the synthesis of $\beta$-$NaYF_4$, but the as-prepared products usually have less uniformity and broad size distribution. Alternatively, the solvothermal method has been proven to be powerful in producing $\beta$-$NaYF_4$ UCNCs of small size, high uniformity, monodispersity and bright UCL. However, to achieve a desired size, crystal phase and excellent optical properties of UCNCs using the above-mentioned methods it is necessary to control simultaneously a set of experimental parameters such as reaction temperature, time, solvent and concentration of precursors. To simplify the synthetic procedure, Liu *et al.* reported the rational control of the size and phase of $NaYF_4$ NCs by $Gd^{3+}$ doping, but the influence of $Gd^{3+}$ on the UV UCL in small-sized $\beta$-$NaYF_4$:Yb,Tm,Gd NCs was not reported.[27] Qin *et al.* first investigated the use of $Gd^{3+}$ in $Yb^{3+}$-$Tm^{3+}$-$Gd^{3+}$

coexisting nanoparticles and reported the shortest UV UCL.[28] However, the less uniformity and large size of the nanoparticles may limit their potential applications. Notably, different host materials doped with the same activator display diverse emission profiles due to distinct energy transfer pathways caused by different dopant-host interactions.[29-31] Therefore, although impressive progress has been made in recent years, the search for new materials and new methods for better UCL performance or desired nanoscale characteristics, especially in small-sized and uniform UCNCs with intense high-order UV UCL, continues to be of great interest.

In this paper, we present a simple method that affords controlled synthesis of large-scale monodisperse $\beta$-$NaYF_4$:$Ln^{3+}$ ($Ln^{3+}$ = $Yb^{3+}$, $Tm^{3+}$, $Gd^{3+}$ or $Ce^{3+}$) UCNCs with a narrow size distribution and intense UV UCL. The approach is based on the strategy of using two co-doped emitting $Ln^{3+}$ and combines the merits of solvothermal method (short reaction time, monodisperse and morphology control) and lanthanide doping strategy (control of the crystallographic phase, size, and morphology). Importantly, the size of $\beta$-$NaYF_4$ UCNCs can be modulated from 25 nm down to 8 nm by adjusting the concentration of the co-doped $Gd^{3+}$ or $Ce^{3+}$ while preserving the $\beta$ phase of the nanocrystals. Even the ultra-small, 8 nm-diameter nanoparticles still exhibit appreciable UC emissions in the UV region upon NIR excitation. Using the 8 nm-diameter UCNCs, we also synthesized and characterized more efficient UC core-shell structures as small as 12 nm in diameter.

## Experimental Section

### Chemicals

All chemicals were of analytical grade and used without further purification. $YCl_3·6H_2O$ (99.999%), $YbCl_3·6H_2O$ (99.999%), $TmCl_3·6H_2O$ (99.999%), $GdCl_3·6H_2O$ (99.99%), $CeCl_3·6H_2O$ (99.99%), were purchased from Shandong Yutai Chemical Reagent Company. NaOH (98%), $NH_4F$ (98%), 1-octadecene (ODE, 90%) and oleic acid (OA, 90%) were purchased from Sigma-Aldrich.

### Synthesis of Nanocrystals

**Synthesis of $NaYF_4$:18%Yb,0.5%Tm**

In a typical procedure, 1 mmol $RECl_3·6H_2O$ (RE = 81.5 mol% Y, 18 mol% Yb, 0.5 mol% Tm) was dissolved in a mixture of ODE (15 mL) and OA (6 mL). The solution was heated to 160 °C for 30 min under argon protection to form the lanthanide oleate complexes. The solution was then cooled to room temperature with a gentle flow of argon gas through the reaction flask. During this time, a solution of $NH_4F$ (4 mmol) and NaOH (2.5 mmol) dissolved in methanol (10 mL) was added to the flask and the resulting mixture was stirred for 30 min. The temperature was then increased to 50 °C for evaporating methanol from the reaction mixture; in succession, the solution was heated to 300 °C in an argon atmosphere for 60 min and then cooled to room temperature naturally. The resulting solid products were precipitated by addition of ethanol, collected by centrifugation at 10000 rpm for 10 min, washed with ethanol three times, and finally re-dispersed in hexane for further experiments.

**Synthesis of $NaYF_4$:18%Yb,0.5%Tm,X%Gd and $NaYF_4$:18%Yb,0.5%Tm,W%Ce**

The procedures for the synthesis of $NaYF_4$:18%Yb,0.5%Tm,X%Gd NCs and $NaYF_4$:18%Yb,0.5%Tm,W%Ce NCs were similar to those described above, except different amounts of new lanthanide ions ($GdCl_3·6H_2O$, $CeCl_3·6H_2O$) were added.

**Synthesis of core-shell $\beta$-$NaYF_4$:18%Yb,0.5%Tm,20%Gd@ $NaGdF_4$**

0.5 mmol $GdCl_3·6H_2O$ was added to a 100 mL flask containing 6 mL of oleic acid and 15 mL of 1-octadecene and heated to 160 °C under argon gas flow with constant stirring for 1 h to form a clear solution. It was then cooled to 80 °C. Afterwards, 1 mmol $NaYF_4$:18%Yb,0.5%Tm,20%Gd NCs in 6 mL of hexane was added to the above solution and stirred for 30 min. After the removal of hexane, 10 mL of methanol solution containing 2 mmol of $NH_4F$ and 1.25 mmol of NaOH was added and stirred at 50 °C for 30 min. After methanol was evaporated, the solution was heated to 300 °C under argon gas flow with vigorous stirring for 1 h and then cooled to room temperature. The obtained core/shell NCs were precipitated by addition of ethanol, collected by centrifugation at 10000 rpm for 10 min, washed with ethanol three times, and finally re-dispersed in hexane for further experiments.

### Characterizations

The phase identification was performed by X-ray diffraction (XRD) (Model Rigaku RU-200b), using nickel-filtered Cu-Ka radiation (λ = 1.5406 Å). The step scan covered the angular range from 2 theta = 10° to 70° in steps of 0.02°. Transmission electron microscopy (TEM, Hitachi H-7500) images were obtained with an acceleration voltage of 80 kV. Upconversion emission spectra of the samples were recorded with a double-monochromator Fluorolog 2 instrument from Spex. A power-adjustable 980 nm laser diode (MDL-H-980 nm-4W, Changchun New Industies Optoelectronics Tech. Co., Ltd.) was employed as the upconversion pump source. A Raman shift laser running at 953.6 nm (pumped by the second harmonic of a Nd:YAG plused laser) was used as the pulsed excitation source for temporal investigations. The infrared spectra were acquired on a Bomen FT-IR spectrometer (MB 104PH) equipped with a base line-diffused reflectance.

## Results and discussion

The crystal structures and phase purity of the as-prepared products were first examined by X-ray powder diffraction (XRD) (Fig.1). Without $Gd^{3+}$ ions added, the XRD pattern of $NaYF_4$:18%Yb,0.5%Tm NCs can be indexed as pure $\beta$-$NaYF_4$ (JCPDS No. 28-1192) and no diffraction peaks corresponding to impurities were detected. Upon doping with $Gd^{3+}$ ions at various concentrations, the diffractions display no extra peaks, indicating that the presence of $Gd^{3+}$ ions with the used doping levels did not induce phase transformation in the nanocrystals of $NaYF_4$:18%Yb,0.5%Tm,X%Gd (X = 2.5, 7.5, and 20 mol%). This result can be attributed to the small structural difference between $\beta$-$NaYF_4$ and $\beta$-$NaGdF_4$. Importantly, it is visible that with increasing the $Gd^{3+}$ dopant concentration, the diffraction peaks are broadened, indicating decrease in the size of the $\beta$-

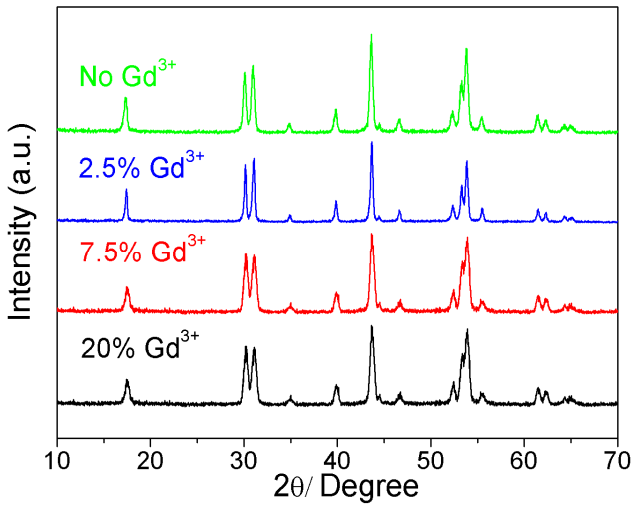


**Fig. 1** XRD patterns of the $NaYF_4$:18%Yb,0.5%Tm,X%Gd NCs with different $Gd^{3+}$ doping contents (X = 0, 2.5, 7.5, and 20 mol%).

$NaYF_4$ NCs. We also investigated the influence of the $Ce^{3+}$ ions doping on the phase of $NaYF_4$:18%Yb,0.5%Tm NCs with varying concentrations of $Ce^{3+}$ ions (5-20 mol%). Similar results were obtained as can be seen from the XRD patterns (Fig.S1, ESI†). A single $\beta$-phase was obtained with increasing the $Ce^{3+}$ content up to 20 mol%, in contrast with a recent report.[32] Moreover, the surface functional groups attached on the $\beta$-$NaYF_4$:$Ln^{3+}$ NCs were identified with FT-IR measurements (Fig.S2, ESI†). Due to the presence of oleic acid molecules, these NCs can be well dispersed into a nonpolar solvent (e.g., cyclohexane, hexane and chloroform) leading to transparent solution.

Adding $Gd^{3+}$ ions in $\beta$-$NaYF_4$:18%Yb,0.5%Tm as a second emitter has as effect to reduce the size of the resulting UCNCs. This is clearly seen from the TEM images in Fig. 2. In the absence of $Gd^{3+}$ ions, the $\beta$-$NaYF_4$:18%Yb,0.5%Tm NCs have an average size of 25 nm (Fig. 2A). After adding $Gd^{3+}$ ions, the size decreases. Indeed, with increasing the $Gd^{3+}$ dopant concentration from 2.5 to 7.5 to 20 mol%, the average size of the $\beta$-$NaYF_4$:18%Yb,0.5%Tm,X%Gd NCs decreases continuously from 20 nm to 15 nm to 8 nm, respectively (Fig. 2B-2D). The smallest 8 nm UCNCs obtained with 20 mol% of $Gd^{3+}$ remain highly uniform. The explanation for the reduced size by incorporating $Gd^{3+}$ ions is known.[27] By substituting smaller $Y^{3+}$ ions (1.159 Å) by larger $Gd^{3+}$ ions (1.193 Å),[33] the electron charge density of the crystal surface is increased. This change can slow down the diffusion of negatively changed $F^-$ ions to the surface due to increased charge repulsion, resulting in a reduction of the $\beta$-$NaYF_4$ NCs size. By increasing the amount of $Gd^{3+}$ ions, such size reduction effect becomes more prominent. Following the same line of thought, we also investigated the use of $Ce^{3+}$ ions doping to reduce the size of UCNCs. TEM observations found that pure $\beta$-$NaYF_4$:18%Yb,0.5%Tm,W%Ce NCs with W% = 5, 10, and 20 mol%, were formed under our used conditions, giving rise to NCs having an average size of 28, 18, and 10 nm, respectively (Fig.S3, ESI†). The homogeneity of the UCNCs over a large area can be appreciated from a low magnification TEM image (Fig. S4, ESI†). This result contracts with some previous reports showing that increasing the $Ce^{3+}$ dopant content may lead

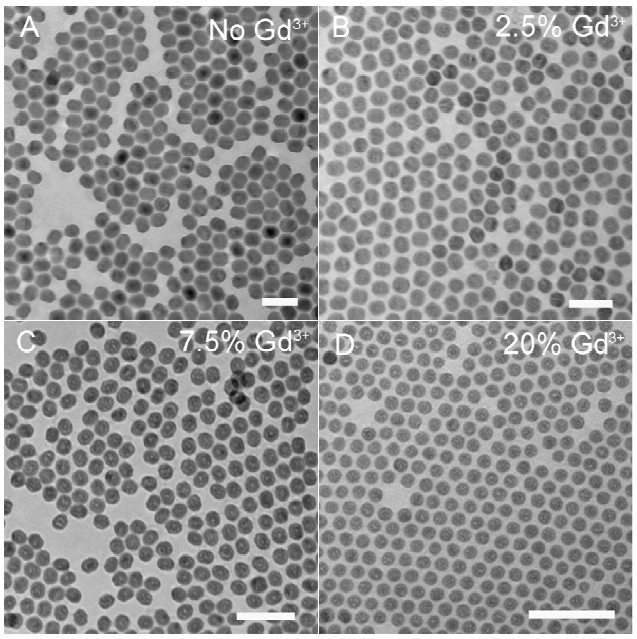


**Fig. 2** TEM images of $\beta$-$NaYF_4$:18%Yb,0.5%Tm,X%Gd NCs with various concentrations of $Gd^{3+}$: (A) no $Gd^{3+}$, (B) 2.5 mol% $Gd^{3+}$, (C) 7.5 mol% $Gd^{3+}$ and (D) 20 mol% $Gd^{3+}$. Scale bars = 50 nm.

to the formation of anisotropic $NaYF_4$ NCs in the form of nanorods or crystals of mixed phases ($\alpha$ and $\beta$) due to the large difference in the ionic radii between $Y^{3+}$ ions (1.159 Å) and $Ce^{3+}$ ions (1.283 Å).[32-34]

Although extra-small NCs of $\beta$-$NaYF_4$:18%Yb,0.5%Tm,X%Gd were obtained, for the specific application mentioned above, i.e., nano-scale UV light source upon NIR excitation, efficient UCL in the UV region is required.[12-14,35] The photoluminescence behavior of $\beta$-$NaYF_4$:18%Yb,0.5%Tm,X%Gd NCs upon 980 nm excitation was thus investigated. The recorded photoluminescence spectra are given in Fig. 3 for UCNCs of various sizes, the NCs without $Gd^{3+}$ dopant (25 nm) being also shown for comparison. The spectra were all recorded under the same conditions (emission slit is 0.5 nm, 400 V high voltages of the photomultiplier tube, and the excitation power density set at about 100 W $cm^{-2}$). All the emissions of $Tm^{3+}$ and $Gd^{3+}$ match very well with previous reports.[28] Several characteristic high-order UC emissions in the UV region from both $Tm^{3+}$ and $Gd^{3+}$ are visible. As indicated in the figure, these transitions are $^6I_J \rightarrow {}^8S_{7/2}$ (270-281 nm, $Gd^{3+}$), $^1I_6 \rightarrow {}^3H_6$ (291 nm, $Tm^{3+}$), $^6P_{5/2} \rightarrow {}^8S_{7/2}$ (305 nm, $Gd^{3+}$), $^6P_{7/2} \rightarrow {}^8S_{7/2}$ (311 nm, $Gd^{3+}$), $^1I_6 \rightarrow {}^3F_4$ (345 nm, $Tm^{3+}$), and $^1D_2 \rightarrow {}^3H_6$ (363 nm, $Tm^{3+}$). Among the emitted UV photons, those at emission wavelengths between 340 and 365 nm are most useful for activating UV-sensitive materials by NIR excitation. Although the emission intensity decreases with decreasing the size of UCNCs, an appreciable amount remains even for the 8 nm NCs. The inset of Fig. 3 is an enlarged area for emissions below 330 nm. In addition to the peak at 290 nm from $Tm^{3+}$ that is the most intense for the UCNCs without $Gd^{3+}$ ions, the characteristic emissions from $Gd^{3+}$ ions at shorter and longer wavelengths are observable for UCNCs doped by $Gd^{3+}$. We are not aware of previous reports of intense UV and high-order UV UC emissions in NCs of such small sizes.

Fig.4 describes the energy level diagrams of $Yb^{3+}$, $Tm^{3+}$, and

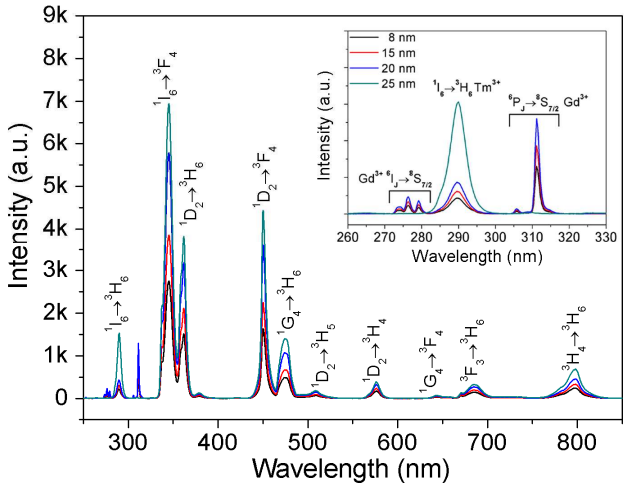


**Fig. 3** UCL spectra of $\beta$-$NaYF_4$:18%Yb,0.5%Tm,X%Gd NCs of various sizes upon 980 nm excitation. The inset shows an enlarged area of the spectra in part of the UV region (260-330 nm).

$Gd^{3+}$ and the possible UC processes under 980 nm excitation. In $Yb^{3+}$-$Tm^{3+}$-$Gd^{3+}$ tridoped systems, $Yb^{3+}$ acts as the sensitizer that absorbs the 980 nm NIR light and successively transfers energy to $Tm^{3+}$ to populate its $^3H_5$, $^3F_{2,3}$ and $^1G_4$ levels.[36] The $^1D_2$ level of $Tm^{3+}$ cannot be populated directly via an energy transfer (ET) from excited $Yb^{3+}$ due to a large energy mismatch (about 3500 $cm^{-1}$). Instead, the $^1D_2$ level, which is responsible for 4-photon UCL, is populated via the cross relaxation $^3F_3 + {}^3H_4 \rightarrow {}^3H_6 + {}^1D_2$ between $Tm^{3+}$ ions. Then, from $^1D_2$ the $^3P_2$ level of $Tm^{3+}$ is populated by another ET $^2F_{5/2} \rightarrow {}^2F_{7/2}$ ($Yb^{3+}$):$^1D_2 \rightarrow {}^3P_2$ ($Tm^{3+}$) and then relaxes rapidly to the $^1I_6$ state, which accounts for the 5-photon UCL of $Tm^{3+}$. The details in the energy level population and transition processes are depicted in Fig.4. Therefore, upon 980 nm excitation, UCL of $Tm^{3+}$ corresponding to the various electronic transitions can be observed, including the most prominent UV ($^1I_6 \rightarrow {}^3H_6$, $^1I_6 \rightarrow {}^3F_4$, and $^1D_2 \rightarrow {}^3H_6$) and blue emissions ($^1D_2 \rightarrow {}^3F_4$ and $^1G_4 \rightarrow {}^3H_6$). On the other hand, owing to the large energy gap between the ground state $^8S_{7/2}$ and the first excited states $^6P_J$, the $Gd^{3+}$ cannot absorb 980 nm photons directly. However, in $Yb^{3+}$-$Tm^{3+}$-$Gd^{3+}$ tridoped systems, the excited $Tm^{3+}$ in the $^3P_2$ level can transfer energy to $Gd^{3+}$ to promote its excitation through ET $^3P_2 \rightarrow {}^3H_6$ ($Tm^{3+}$):$^8S_{7/2} \rightarrow {}^6I_J$

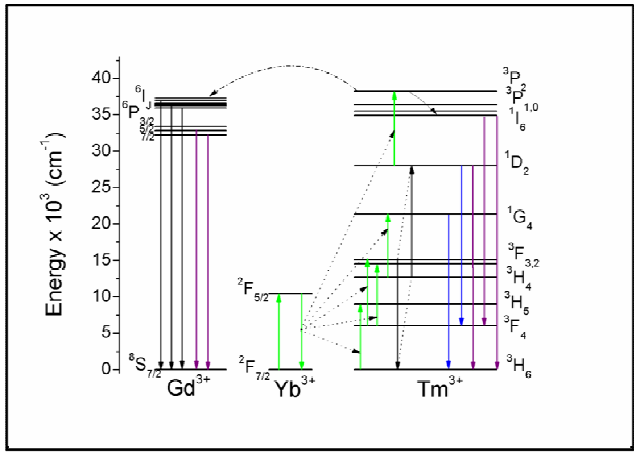


**Fig. 4** Schematic energy level diagrams of $Yb^{3+}$, $Tm^{3+}$, $Gd^{3+}$, and possible UC emission processes.

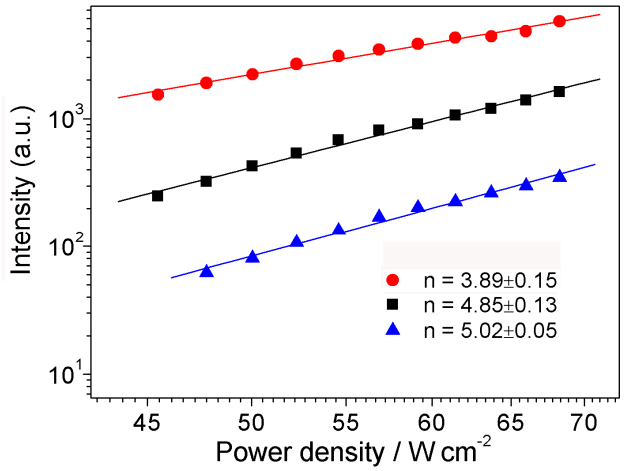


**Fig. 5** Plot (log-log) of UC emission intensity versus excitation power in $\beta$-$NaYF_4$:18%Yb,0.5%Tm,20%Gd NCs for three emissions at 311 nm (triangle symbol), 345 nm(square) and 363 nm (sphere).

($Gd^{3+}$). In other words, $Tm^{3+}$ acts as sensitizer for $Gd^{3+}$. At room temperature, the nonradiative relaxation probability of excited $Gd^{3+}$ through $^6I_J \rightarrow {}^6P_J$ is higher than the radiative transition probability of $^6I_{7/2} \rightarrow {}^8S_{7/2}$. This results in populating the $^6P_{5/2}$ and $^6P_{7/2}$ levels efficiently, from where high-order UV emissions of $Gd^{3+}$ can be observed via the transitions of $^6I_J \rightarrow {}^8S_{7/2}$ and $^6P_J \rightarrow {}^8S_{7/2}$, respectively.[28]

Direct evidence of energy transfer from $Tm^{3+}$ to $Gd^{3+}$ in our UCNCs can also be found by comparing the UC emission spectra of $\beta$-$NaYF_4$:18%Yb,0.5%Tm to that of $\beta$-$NaYF_4$:18%Yb,0.5%Tm,X%Gd NCs (inset of $^1I_6 \rightarrow {}^3H_6$ Fig. 3). Upon addition of $Gd^{3+}$ in the NCs, the 5-photon UCL peaks of $Tm^{3+}$ ($^1I_6 \rightarrow {}^3H_6$ and $^1I_6 \rightarrow {}^3F_4$) display reduced intensities. As the concentration of $Gd^{3+}$ increases, these two UV emission peaks of $Tm^{3+}$ decreases drastically. Moreover, as seen from the excitation power dependence of UCL of $\beta$-$NaYF_4$:18%Yb,0.5%Tm,20%Gd NCs (Fig. S5, ESI†), although all peaks become more prominent with increasing the excitation power, the emission intensity in the UV region increases relative to the emission in the NIR region. This is shown by the increase in the fluorescence branching ratio of $I_{345}/I_{798}$ as a function of the excitation power (inset in Fig. S5).

Other experiments were performed to further confirm the *n*-photon UC processes. For an unsaturated UC process, the emission intensity is proportional to the $n^{th}$ power of the excitation intensity and the integer $n$ is the number of the laser photons absorbed per upconverted photon emitted. Fig. 5 shows the typical pump-power dependence of the UC luminescence of $\beta$-$NaYF_4$:18%Yb,0.5%Tm,20%Gd NCs: $n$ = 5.02 ± 0.05, 4.85 ± 0.13, and 3.89 ± 0.15 for the UV UC emissions at 311 nm, 345 nm, and 363 nm, respectively. The results means that the populations of the states $^6P_{7/2}$, $^1I_6$, and $^1D_2$ came from five-photon, five-photon, and four-photon UC processes, respectively.

The overall UV emissions intensity of the NCs decreases with increasing the $Gd^{3+}$ dopant content, which is primarily attributed to the reduction in the size of NCs. Smaller NCs tend to increase surface quenching sites and enhance nonradiative energy transfer processes of the lanthanide ions, which suppress UCL. In order to improve the photoluminescence intensity of the UCNCs, two-step solvothermal method was selected to produce core/shell $\beta$-$NaYF_4$:18%Yb,0.5%Tm,20%Gd@$NaGdF_4$ NCs, using the 8 nm

NCs as the core. Notably, heterogeneous shell ($NaGdF_4$) not only efficiently enhances the intensity of upconversion emissions but also incorporates new functionalities. In the present case, the $Gd^{3+}$-based core/shell UCNCs can be used as dual-modality contrast agent for magnetic resonance imaging (MRI) and optical imaging, and, due to $Gd^{3+}$ doped UCNCs with higher atomic

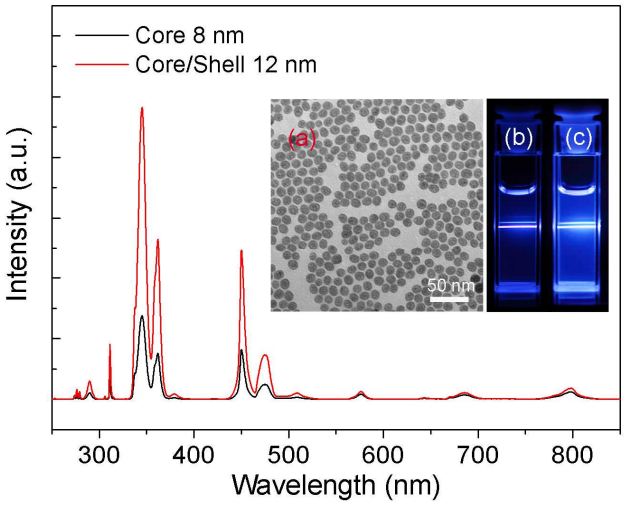


**Fig. 6** UCL spectra of the NCs of $\beta$-$NaYF_4$:18%Yb,0.5%Tm,20%Gd (core) and $\beta$-$NaYF_4$:18%Yb,0.5%Tm,20%Gd@$NaGdF_4$ (core/shell). Inset: (a) TEM image of $\beta$-$NaYF_4$:18%Yb,0.5%Tm,20%Gd@$NaGdF_4$ NCs, and pictures of (b) a dispersion of the core NCs and (c) a dispersion of the core-shell NCs in hexane (~ 1 wt%) exposed to a 980 nm diode laser.

number and stronger X-ray attenuation, can also be served as computed tomography (CT) contrast agents.[37-40] Fig. 6 compares the UCL spectra of the core/shell NCs with the core of $\beta$-$NaYF_4$:18%Yb,0.5%Tm,20%Gd NCs. The improved UCL of the core/shell NCs is visible. In the inset of Fig. 6, the more intense UCL of the core/shell NCs with respect to the core NCs can also be seen from the photos of the NCs dispersions in hexane (~ 1 wt%) upon passage of a 980 nm laser, while the TEM image of the core/shell NCs reveals an average diameter of 12 nm. The result shows that small and intense UV UC core/shell NCs can be prepared by growing a shell around the 8 nm NCs. In order to better verify the UCL enhancement, we also compared the core/shell and core NCs by dynamic analysis of $Gd^{3+}$ and $Tm^{3+}$ excited states. The decay curves for the representative emissions from the $^6P_{7/2}$ level of $Gd^{3+}$ and $^1I_6$ level of $Tm^{3+}$ were recorded under 953.6 nm pulsed Raman shift laser, as shown in Fig. 7. Each of the decay curves can be fitted well into a single-exponential function as $I = I_0\exp(-t/\tau)$, where $I_0$ is an intensity parameter and $\tau$ is the lifetime of the monitored excited state. As can be seen from Fig. 7, all the lifetimes of the $^6P_{7/2}$ level of $Gd^{3+}$ and $^1I_6$ level of $Tm^{3+}$ are longer in the core/shell NCs than in the core NCs. For UC materials, a longer lifetime usually means a more efficient UCL. Therefore, the results on the UCL dynamic analysis further confirm a significant increase in the intensity of the UCL for the core-shell UCNCs.

## Conclusions

In summary, we successfully synthesized ultra-small, monodisperse, and highly uniform $\beta$-$NaYF_4$:$Ln^{3+}$ ($Ln^{3+}$ = $Yb^{3+}$, $Tm^{3+}$, $Gd^{3+}$ or $Ce^{3+}$) UCNCs by using the solvothermal method. By varying the $Gd^{3+}$ ions dopant content (X%), the controlled synthesis of $\beta$-$NaYF_4$:18%Yb,0.5%Tm,X%Gd NCs was realized, resulting in UCNCs of varying sizes ranging from 8 nm to 25 nm in diameter. Intense and high-order UV UC emissions from UCNCs of such small sizes were reported, for the first time to our

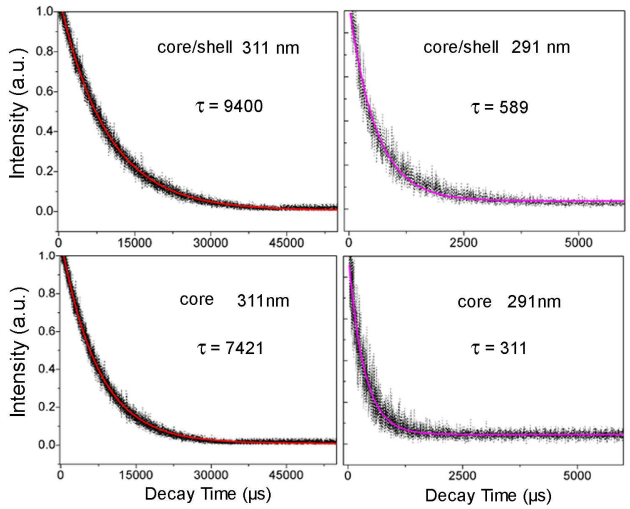


**Fig. 7** Temporal evolution of UC luminescence from the $^6P_{7/2}$ level of $Gd^{3+}$ and $^1I_6$ level of $Tm^{3+}$ in both the core/shell and the core NCs under the excitation of 953.6 nm pulsed Raman shift laser: experimental data (black line) and fitting by $I = I_0\exp(-t/\tau)$ (colored line).

knowledge. Moreover, using the 8 nm UCNCs, heterogeneous core/shell NCs of $\beta$-$NaYF_4$:18%Yb,0.5%Tm,20%Gd@$NaGdF_4$ of 12 nm were also prepared, displaying more efficient UV UCL than the 8 nm core NCs. Ultra-small UCNCs with efficient UV emission upon NIR excitation are particularly useful for loading in UV-sensitive polymer nanocarriers for NIR-controlled drug release and other biomedical applications.

## Acknowledgements

We acknowledge the natural support from the Natural Science and Engineering Research Council of Canada (NSERC), Le Fonds de recherche du Quebec: nature et technologies (FRQNT). YZ is a member of FRQNT-funded Center for Self-Assembled Chemical Structures (CSACS) and Centre quebecois sur les materiaux fonctionnels (CQMF). YS thanks Paul-Ludovic Karsenti (Universite de Sherbrooke) and Dr. Weiye Song (Jilin University) for UCL and dynamic photoluminescence measurements.

## Notes and references

*Département de chimie, Université de Sherbrooke, Sherbrooke, Québec, Canada J1K 2R1. Fax: 819-8218017; Tel: 819-8217090; E-mail: yue.zhao@usherbrooke.ca*

† Electronic Supplementary Information (ESI) available: [details of any supplementary information available should be included here]. See DOI: 10.1039/b000000x/

1 F. Auzel, *Chem. Rev.*, 2004, **104**, 139-173.

2 F. Wang and X. G. Liu, *Chem. Soc. Rev.*, 2009, **38**, 976-989.

3 Z. J. Gu, L. Yan, G. Tian, S. J. Li, Z. F. Chai and Y. L. Zhao, *Adv. Mater.*, 2013, **25**, 3758-3779.

4 H. H. Gorris and O. S. Wolfbeis, *Angew. Chem. Int. Ed.*, 2013, **52**, 3584-3600.

5 F. Wang and X. G. Liu, *J. Am. Chem. Soc.*, 2008, **130**, 5642-5643.
6 Z. Q. Li, Y. Zhang and S. Jiang, *Adv. Mater.*, 2008, **20**, 4765-4769.
7 S. Wu, G. Han, D. J. Milliron, S. Aloni, V. Altoe, D. V. Talapin, B. E. Cohen and P. J. Schuck, *Proc. Natl. Acad. Sci. U.S.A.*, 2009, **106**, 10917-10921.
8 G. Y. Chen, C. H. Yang and P. N. Prasad, *Acc. Chem. Res.*, 2013, **46**, 1474-1486.
9 W. P. Qin, D. S. Zhang, D. Zhao, L. L. Wang and K. Z. Zheng, *Chem. Commun.*, 2010, **46**, 2304-2306.
10 D. K. Chatterjee and Y. Zhang, *Nanomedicine-Uk*, 2008, **3**, 73-82.
11 G. Y. Chen, J. Shen, T. Y. Ohulchanskyy, N. J. Patel, A. Kutikov, Z. P. Li, J. Song, R. K. Pandey, H. Ågren, P. N. Prasad and G. Han, *Acs Nano*, 2012, **6**, 8280-8287.
12 B. Yan, J.-C. Boyer, N. R. Branda and Y. Zhao, *J. Am. Chem. Soc.*, 2011, **133**, 19714-19717.
13 B. Yan, J.-C. Boyer, D. Habault, N. R. Branda and Y. Zhao, *J. Am. Chem. Soc.*, 2012, **134**, 16558-16561.
14 M. L. Viger, M. Grossman, N. Fomina and A. Almutairi, *Adv. Mater.*, 2013, **25**, 3733-3738.
15 D. K. Chatterjee, L. S. Fong and Y. Zhang, *Adv. Drug. Deliver. Rev.*, 2008, **60**, 1627-1637.
16 C. Wang, H. Tao, L. Cheng and Z. Liu, *Biomaterials*, 2011, **32**, 6145-6154.
17 S. F. Lim, R. Riehn, W. S. Ryu, N. Khanarian, C.-K. Tung, D. Tank and R. H. Austin, *Nano. Lett.*, 2005, **6**, 169-174.
18 F. Shi, J. S. Wang, X. S. Zhai, D. Zhao and W. P. Qin, *Crystengcomm*, 2011, **13**, 3782-3787.
19 X. Teng, Y. Zhu, W. Wei, S. Wang, J. Huang, R. Naccache, W. Hu, A. I. Y. Tok, Y. Han, Q. Zhang, Q. Fan, W. Huang, J. A. Capobianco and L. Huang, *J. Am. Chem. Soc.*, 2012, **134**, 8340-8343.
20 Y. Ding, X. Teng, H. Zhu, L. Wang, W. Pei, J.-J. Zhu, L. Huang and W. Huang, *Nanoscale*, 2013, **5**, 11928-11932.
21 J. H. Zeng, J. Su, Z. H. Li, R. X. Yan and Y. D. Li, *Adv. Mater.*, 2005, **17**, 2119-2123.
22 C. Zhang and J. Chen, *Chem. Commun.*, 2010, **46**, 592-594.
23 D. K. Ma, D. P. Yang, J. L. Jiang, P. Cai and S. M. Huang, *Crystengcomm*, 2010, **12**, 1650-1658.
24 X. C. Ye, J. E. Collins, Y. J. Kang, J. Chen, D. T. N. Chen, A. G. Yodh and C. B. Murray, *Proc. Natl. Acad. Sci. U.S.A.*, 2010, **107**, 22430-22435.
25 Z. Q. Li and Y. Zhang, *Nanotechnology*, 2008, **19**.
26 M. Wang, C. C. Mi, S. Wang, F. Li, J. L. Liu and S. K. Xu, *Spectrosc. Spect. Anal.*, 2009, **29**, 3327-3331.
27 F. Wang, Y. Han, C. S. Lim, Y. H. Lu, J. Wang, J. Xu, H. Y. Chen, C. Zhang, M. H. Hong and X. G. Liu, *Nature*, 2010, **463**, 1061-1065.
28 C. Y. Cao, W. P. Qin, J. S. Zhang, Y. Wang, P. F. Zhu, G. D. Wei, G. F. Wang, R. J. Kim and L. L. Wang, *Opt. Lett.*, 2008, **33**, 857-859.
29 J. Wang, F. Wang, C. Wang, Z. Liu and X. G. Liu, *Angew. Chem. Int. Ed.*, 2011, **50**, 10369-10372.
30 G. Tian, Z. J. Gu, L. J. Zhou, W. Y. Yin, X. X. Liu, L. Yan, S. Jin, W. L. Ren, G. M. Xing, S. J. Li and Y. L. Zhao, *Adv. Mater.*, 2012, **24**, 1226-1231.
31 Y. Zhang, J. D. Lin, V. Vijayaragavan, K. K. Bhakoo and T. T. Y. Tan, *Chem. Commun.*, 2012, **48**, 10322-10324.
32 H. Na, K. Woo, K. Lim and H. S. Jang, *Nanoscale*, 2013, **5**, 4242-4251.
33 R. Shannon, *Acta. Cryst.*, 1976, **A32**, 751-767.
34 X. F. Yu, M. Li, M. Y. Xie, L. D. Chen, Y. Li and Q. Q. Wang, *Nano. Res.*, 2010, **3**, 51-60.
35 T. Q. Wu, M. Barker, K. M. Arafeh, J.-C. Boyer, C.-J. Carling and N. R. Branda, *Angew. Chem. Int. Ed.*, 2013, **52**, 11106-11109.
36 G. F. Wang, W. P. Qin, L. L. Wang, G. D. Wei, P. F. Zhu and R. J. Kim, *Opt. Express.*, 2008, **16**, 11907-11914.
37 Y. Hou, R. R. Qiao, F. Fang, X. X. Wang, C. Y. Dong, K. Liu, C. Y. Liu, Z. F. Liu, H. Lei, F. Wang and M. Y. Gao, *Acs Nano*, 2012, **7**, 330-338.
38 H. Y. Xing, W. B. Bu, S. J. Zhang, X. P. Zheng, M. Li, F. Chen, Q. J. He, L. P. Zhou, W. J. Peng, Y. Q. Hua and J. L. Shi, *Biomaterials*, 2012, **33**, 1079-1089.
39 X. J. Zhu, J. Zhou, M. Chen, M. Shi, W. Feng and F. Y. Li, *Biomaterials*, 2012, **33**, 4618-4627.
40 S. J. Zeng, J. J. Xiao, Q. B. Yang and J. H. Hao, *J. Mater. Chem.*, 2012, **22**, 9870-9874.

# Sub-10 nm and monodisperse $\beta$-$NaYF_4$:Yb,Tm,Gd nanocrystals with intense ultraviolet upconversion luminescence

**Feng Shi and Yue Zhao***

Lanthanide-doped upconversion nanocrystals of $\beta$-$NaYF_4$:18%Yb,0.5%Tm,X%Gd and core/shell structured $\beta$-$NaYF_4$:18%Yb,0.5%Tm,20%Gd@$NaGdF_4$ as small as 8 nm and 12 nm in diameter respectively, were synthesized. They display intense and high-order ultraviolet (UV) emissions upon 980 nm excitation, making them particularly attractive for loading in UV-degradable polymer nanocarriers as inside UV light source under near infrared (NIR) light excitation.